The $Yb_2Al_{1-x}Mg_xSi_2$ series from a spin fluctuation ($x = 0$) to a magnetically ordered ground state ($x = 1$)

2009 J. Phys.: Condens. Matter 21 176001

(http://iopscience.iop.org/0953-8984/21/17/176001)

J. Phys.: Condens. Matter **21** (2009) 176001 (8pp) doi:10.1088/0953-8984/21/17/176001

The $Yb_2Al_{1-x}Mg_xSi_2$ series from a spin fluctuation ($x = 0$) to a magnetically ordered ground state ($x = 1$)

K V Shah[1], P Bonville[2], P Manfrinetti[3,4], F Wrubl[3] and S K Dhar[1]

[1] Department of Condensed Matter Physics and Materials Science, Tata Institute of Fundamental Research, Homi Bhabha Road, Navy Nagar, Mumbai 400005, India
[2] Commissariat à l'Energie Atomique, Centre de Saclay, DSM/SPEC, F-91191 Gif-sur-Yvette, France
[3] Dipartimento di Chimica e Chimica Industriale, Università di Genova, Via Dodecaneso 31, I-16146 Genova, Italy
[4] LAMIA Laboratory-CNR-INFM, Corso Perrone 24, I-16152 Genova, Italy

Received 23 October 2008, in final form 5 February 2009
Published 24 March 2009
Online at stacks.iop.org/JPhysCM/21/176001

Abstract

The structural and magnetic properties of $Yb_2Al_{1-x}Mg_xSi_2$ ($x = 0$, 0.5 and 1), crystallizing in the tetragonal Mo_2FeB_2-type structure, are reported in this work. Yb_2AlSi_2 exhibits a Pauli paramagnetic ground state arising due to spin/valence fluctuations induced by a significant Yb 4f conduction band hybridization. High-field magnetization (up to 120 kOe) indicates a nearly temperature-independent susceptibility of 8.6×10^{-3} emu/Yb mol below 10 K. On the other hand, Yb ions in Yb_2MgSi_2 order antiferromagnetically at a relatively high temperature T_N of 9.5 K. The intermediate composition alloy $Yb_2Al_{0.5}Mg_{0.5}Si_2$ is a Kondo lattice, antiferromagnet with $T_N = 5.5$ K. The coefficient of the linear term of the electronic heat capacity, γ, of Yb_2AlSi_2 is found to be 305 mJ mol^{-1} K^{-2}, indicating a significant electronic mass enhancement due to strong electronic correlations. Below 12 K, an additional contribution to the heat capacity of the form $T^3 \ln T$ is observed. The ^{170}Yb Mössbauer spectra in the ordered state of Yb_2MgSi_2 indicate a strong coupling of the 4f quadrupolar moment with the magnetic moment through a magneto-elastic coupling.

(Some figures in this article are in colour only in the electronic version)

1. Introduction

Yb_2AlSi_2 [1] and Yb_2MgSi_2 [2] are known to form in the tetragonal Mo_2FeB_2-type structure with space group $P4/mbm$, which is a ternary ordered derivative of the U_3Si_2 structure. In the binary prototype, the uranium ions occupy two distinct lattice sites, 4h and 2a, but in the ternary derivative the Yb ions occupy the unique 4h site of the unit cell. This makes these two Yb compounds attractive for an exploration of their magnetic properties as complexities due to a possible site-dependent magnetic response should be absent. The study of Yb-based compounds is important as it enriches our understanding of the strongly correlated electron behavior in metals, arising from an enhanced interaction between the local Yb 4f moment and the conduction electrons.

Yb_2MgSi_2 is one of the members of a series of isostructural compounds of composition R_2MgSi_2 (R = Y, La–Nd, Sm, Gd–Lu). The cell volume of Yb_2MgSi_2 follows the behavior expected on the basis of lanthanide contraction when compared with those of the neighboring analogs and thus suggests a trivalent Hund's-rule-derived $^2F_{7/2}$ state of the Yb ions [2, 3]. On the other hand, in the case of R_2AlSi_2 the analogs with R = Y, Ho, Er, Tm and Lu adopt the orthorhombic W_2CoB_2-type structure and hence the possible magnetic state of the Yb ions in Yb_2AlSi_2 cannot be ascertained from cell volume considerations [1]. In this report we have carried out a detailed study of the magnetic behavior of these two Yb compounds using the techniques of magnetization, heat capacity, electrical resistivity and ^{170}Yb Mössbauer spectroscopy. We find that the Yb^{3+} ions order magnetically in Yb_2MgSi_2 at a relatively high temperature of 9.5 K, when compared with the magnetic ordering temperature of nearly 31 K in isostructural Gd_2MgSi_2. On the other hand, Yb_2AlSi_2 exhibits a Pauli paramagnetic, moderate

Table 1. Lattice constants as obtained by Guinier powder patterns for the compounds $Yb_2Al_{1-x}Mg_xSi_2$ ($x = 0$, 0.5 and 1) and Gd_2MgSi_2 (tetragonal Mo_2FeB_2 type; $tP10$, $P4/mbm$).

		Lattice constants		Unit cell volume
Compound	Heat treatment	a (Å)	c (Å)	V_U (Å^3)
Yb_2AlSi_2	900 °C—11 days 800 °C—9 days	6.7731(4)	4.2403(4)	194.52(5)
$Yb_2Al_{0.5}Mg_{0.5}Si_2$	800 °C—10 days	6.9234(8)	4.1669(6)	199.30(5)
Yb_2MgSi_2	800 °C—6 days	7.0530(6)	4.1282(5)	205.52(8)
Gd_2MgSi_2	800 °C—8 days	7.233(1)	4.2519(7)	221.8(1)

heavy fermion ground state arising from a significant Yb 4f conduction band hybridization. Due to the diametrically opposite nature of the magnetic ground state in these two end members, we also studied $Yb_2Al_{0.5}Mg_{0.5}Si_2$, which orders magnetically at 5.5 K and shows Kondo behavior in the temperature variation of its resistivity.

2. Experimental details

Due to the high vapor pressure of Yb and Mg metal, Yb_2AlSi_2, Yb_2MgSi_2, $Yb_2Al_{0.5}Mg_{0.5}Si_2$ and Gd_2MgSi_2 were prepared in sealed, degassed tantalum crucibles. The metals used were commercial products with high purity (99.9 wt% for the rare earths; 99.99 wt% for aluminum and magnesium; 99.999 wt% for silicon). Weighed amounts of the elements (small pieces for Yb and turnings for Gd freshly prepared from surface-cleaned ingots; Mg and Al in the form of chips and turnings, respectively; fine grains for Si) with a total mass of about 2 g were directly set and slightly pressed together into out-gassed tantalum crucibles; they were sealed by arc welding under a flow of pure argon. Samples were melted by slowly heating the crucibles in a high-frequency induction furnace and the crucibles shaken to ensure homogenization; this procedure was repeated twice. The crucibles were then sealed under vacuum in quartz tubes and annealed in resistance furnaces; the details of the heat treatment are given in table 1. No contamination of the alloys due to reactivity towards the container material (Ta) was noticed.

X-ray analysis was carried out by means of powder diffraction methods; powder patterns were obtained by a Guinier–Stoe camera using Cu Kα radiation ($\lambda = 1.5418$ Å) and pure Si as an internal standard ($a = 5.4308$ Å); the Guinier patterns were indexed with the help of the LAZY-PULVERIX program [4] and the lattice parameters determined by the least-squares methods. Metallographic specimens were prepared by the standard polishing methods of a fragment cut from the bulk samples. Magnetization as a function of temperature and applied magnetic field was measured with a superconducting quantum interference device (Quantum Design) and vibrating sample magnetometers (Oxford Instruments). The heat capacity and electrical resistivity were measured in a physical property measuring system (Quantum Design). ^{170}Yb Mössbauer measurements ($E_0 = 84.3$ keV, $I_g = 0$, $I_e = 2$) were performed with a TmB_{12} γ-ray source mounted on an electromagnet drive with triangular velocity signal (1 mm s^{-1} = 68 MHz).

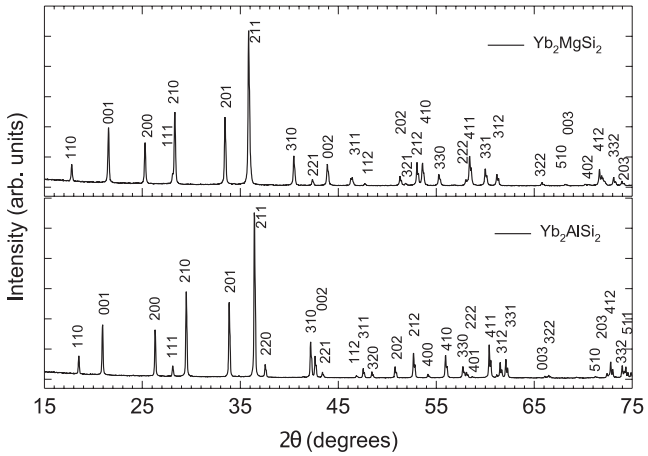

Figure 1. The x-ray powder diffraction patterns of Yb_2MgSi_2 and Yb_2AlSi_2.

3. Results and discussion

3.1. Structure

X-ray powder diffraction patterns of Yb_2AlSi_2 and Yb_2MgSi_2 are shown in figure 1. All the peaks can be indexed to the tetragonal Mo_2FeB_2-type symmetry, showing that the samples are single phase. This is further confirmed by metallographic analysis. In the Gd sample an extra parasitic phase (about 6%), whose exact composition was not determined, was present.

Crystallographic data and lattice constant values of the various compounds are reported in table 1. For $Yb_2Al_{1-x}Mg_xSi_2$ ($x = 0$, 0.5 and 1), the increase of the unit cell volume (which is nearly linear) in passing from the Al ($V_U = 194.52(5)$ Å^3) to the Mg compound ($V_U = 205.52(8)$ Å^3) is expected taking into account the atomic volumes of the elements. It may be noted that the expansion is not isotropic and that the two lattice parameters of the tetragonal Mo_2FeB_2-type unit cell follow opposite trends: the a axis undergoes an expansion while the c axis shows a slight contraction. The near-neighbor atoms of Yb in Yb_2AlSi_2 are 2 Si at 2.845 and 4 Si at 2.956 Å, respectively, followed by 4 Al at 3.267 Å [1]. Therefore, the Yb–Si ligand interaction may be the dominant factor in determining the hybridization experienced by the Yb 4f electronic wavefunctions in these compounds. Al (and Mg) being at the third-nearest-neighbor distance may primarily affect the electronic band structure by the number of valence electrons donated to the conduction band and by their size on the unit cell volume.

3.2. Magnetization

Figure 2 shows the inverse susceptibility χ^{-1} of Yb_2MgSi_2 versus temperature between 1.8 and 300 K in an applied field of 2 kOe. The data present an almost perfect Curie–Weiss law between 300 and 10 K, with the effective moment μ_{eff} of 4.54 μ_B appropriate for Yb^{3+} and a paramagnetic Curie temperature $\theta_p = -35$ K indicative of antiferromagnetic (AF) interactions. The peak at $T_N = 9.5$ K (upper inset, figure 2) signifies the onset of magnetic ordering of the Yb^{3+} moments,

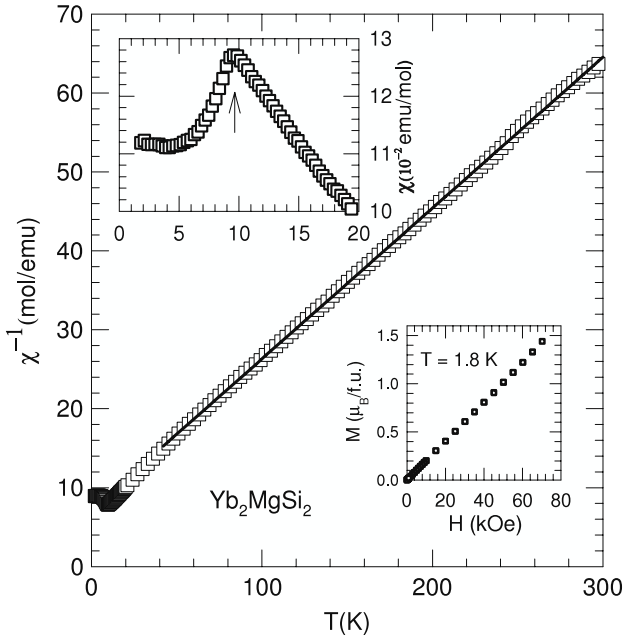

Figure 2. The inverse susceptibility χ^{-1} of Yb_2MgSi_2 between 1.8 and 300 K. The solid line is a fit of the Curie–Weiss law to the data. The upper inset shows χ below 20 K; T_N is indicated by an arrow. The lower inset depicts the in-field magnetization up to 70 kOe at 1.8 K.

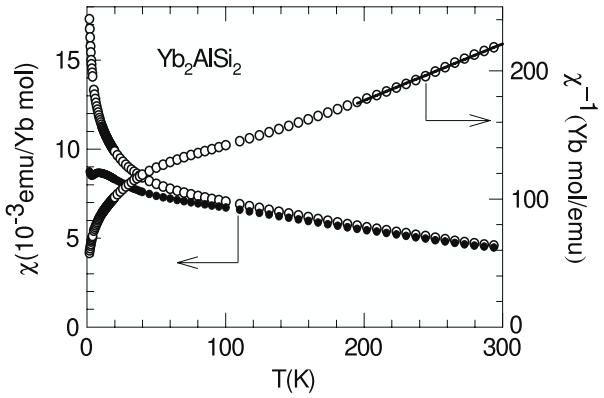

Figure 3. The susceptibility χ and inverse susceptibility χ^{-1} of Yb_2AlSi_2 between 1.8 and 300 K. The solid line is a fit of the Curie–Weiss law to the data. The filled black circles show the likely intrinsic χ of Yb_2AlSi_2 (see the text).

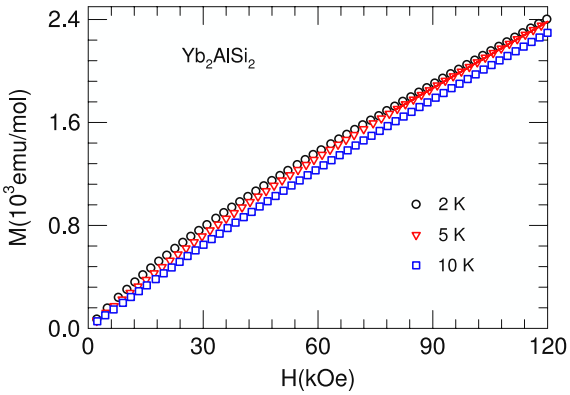

Figure 4. The in-field magnetization of Yb_2AlSi_2 up to 120 kOe at 2, 5 and 10 K. The solid line is a linear fit to the data between 80 and 120 kOe taken at 5 K.

probably with an AF structure. The large value of the ratio $|\theta_p|/T_N \sim 3.5$ points either to the importance of next-nearest-neighbor exchange or to the presence of 4f conduction electron hybridization. The isothermal magnetization at 1.8 K is linear with the field and furnishes a magnetization of nearly 1.5 μ_B per formula unit at the highest applied field of 70 kOe. The variation of the magnetization with field is in conformity with the AF nature of the magnetic transition at 9.5 K.

The magnetic behavior of Yb_2AlSi_2 as probed by magnetization is different. Figure 3 shows χ and χ^{-1} between 1.8 and 300 K. The susceptibility increases monotonically with decreasing temperature, attaining a value of $\sim 17 \times 10^{-3}$ emu/Yb mol at the lowest temperature of 1.8 K. There is no signature of a magnetic transition and the magnetic response in Yb_2AlSi_2 is considerably weaker than in Yb_2MgSi_2. For example, χ of Yb_2MgSi_2 at 15 K in the paramagnetic state is 57×10^{-3} emu/Yb mol compared to the corresponding value of 11.2×10^{-3} emu/Yb mol in Yb_2AlSi_2. Between 200 and 300 K, χ^{-1} of Yb_2AlSi_2 follows nearly a Curie–Weiss behavior with $\mu_{eff} = 4.2\ \mu_B$ and $\theta_p = -203$ K. The large, negative θ_p is a characteristic feature of spin/valence fluctuating Yb compounds in which the strong 4f conduction electron hybridization destabilizes the 4f-derived local moment and gives rise to a Pauli paramagnetic ground state. The weak monotonic increase of the susceptibility at low temperatures in Yb_2AlSi_2 may or may not be intrinsic. In the latter case, Curie-like 'tails' override the temperature-independent susceptibility at low temperatures due to the presence of a tiny fraction of Yb ions in a trivalent electronic state due to the proximity of defects, site exchange, impurities or minor parasitic magnetic phases. Isothermal magnetization was measured up to 120 kOe at 2, 5 and 10 K to probe the variation of the magnetization with field and the data are shown in figure 4. There is a slight curvature in the magnetization at low fields but at higher fields, i.e. above $\sim$70 kOe, a linear response is noted. From the linear portion of the in-field magnetization between 80 and 120 kOe we obtain χ values of 8.54×10^{-3}, 8.6×10^{-3} and 8.65×10^{-3} emu/Yb mol, respectively, at 2, 5 and 10 K. Thus, the high-field magnetization data suggest that the intrinsic susceptibility of Yb_2AlSi_2 is nearly temperature-independent at least below 10 K. Subtracting a constant term of 8.6×10^{-3} emu/Yb mol from the susceptibility data below 10 K of Yb_2AlSi_2, the remaining contribution is accounted for well by a Curie–Weiss description with Curie constant C_{CW} of 0.0354 emu mol^{-1} K^{-1} and $\theta_p = -2.2$ K. If it is assumed that this (extrinsic) contribution is due to Yb^{3+} ions alone, it implies a presence of about 1.5% of trivalent Yb in the sample. The filled black circles in figure 3 show the susceptibility obtained after the contribution calculated from the values of C_{CW} and θ_p is subtracted.

The observation of antiferromagnetic and paramagnetic ground states in the isostructural Yb_2MgSi_2 and Yb_2AlSi_2, respectively, prompted us to probe the magnetic properties at an intermediate composition $Yb_2Al_{0.5}Mg_{0.5}Si_2$. The low-field

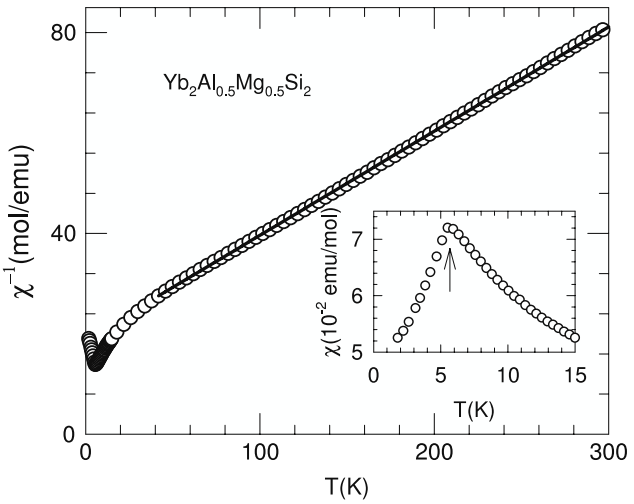

Figure 5. The inverse susceptibility χ^{-1} of $Yb_2Al_{0.5}Mg_{0.5}Si_2$ between 1.8 and 300 K. The solid line is a fit of the Curie–Weiss law to the data. The lower inset shows below χ 15 K; T_N is indicated by an arrow.

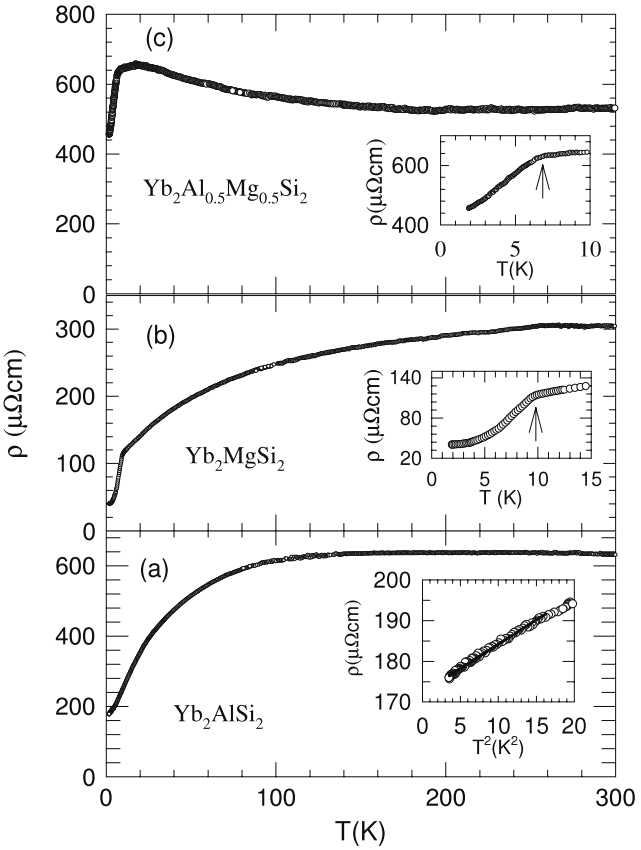

Figure 6. The electrical resistivity ρ of (a) Yb_2AlSi_2; the inset shows the quadratic variation of ρ with temperature T below 4 K, ((b), (c)) Yb_2MgSi_2 and $Yb_2Al_{0.5}Mg_{0.5}Si_2$; the arrows in the insets mark the rapid drop in ρ due to magnetic ordering.

susceptibility taken in an applied field of 50 Oe (lower inset figure 5) shows an AF transition near 5.5 K. The inverse susceptibility measured in a field of 2 kOe, plotted in the main panel, shows Curie–Weiss behavior in an extended range of temperatures similar to Yb_2MgSi_2 with parameters $\mu_{eff} = 4.4\ \mu_B$ and $\theta_p = -91$ K. While μ_{eff} indicates a nearly trivalent state of the Yb ions, which is in conformity with the AF transition at low temperature, a large, negative θ_p signifies an enhanced hybridization between Yb 4f and conduction electrons, lying intermediate between Yb_2AlSi_2 and Yb_2MgSi_2.

3.3. Resistivity

The electrical resistivities of Yb_2AlSi_2, Yb_2MgSi_2 and $Yb_2Al_{0.5}Mg_{0.5}Si_2$ are shown in figure 6. The resistivity of paramagnetic Yb_2AlSi_2 shows a slight negative temperature coefficient between 300 and 200 K and drops gradually below 100 K. Qualitatively, similar behavior has been reported in UAl_2 [5], YbCuAl [6] and some other 4f-and 5f-based spin/valence fluctuation compounds. Evidence for spin/valence fluctuations in Yb_2AlSi_2 due to 4f conduction electron hybridization has been inferred above from the magnetization data. The analysis of the resistivity data at low temperatures reveals that the resistivity follows a quadratic variation (i.e. $\rho = \rho_0 + AT^2$) with $A = 1.195 \times 10^{-6}\ \Omega$ cm. The magnitude of A falls in the range observed for various spin fluctuation and heavy fermion compounds [7].

The electrical resistivity of Yb_2MgSi_2 shows a distinct anomaly at the magnetic transition near 9.5 K. The resistivity decreases rapidly below 9.5 K (see the inset of figure 6(b)) due to the freezing of the spin-disorder-induced scattering of the charge carriers. In the paramagnetic regime the resistivity tends to saturate at high temperatures and qualitatively its thermal variation tends to acquire a character similar to that of Yb_2AlSi_2. We have already remarked above that a negative θ_p of -35 K in Yb_2MgSi_2 may imply a tendency of 4f conduction band hybridization-induced spin fluctuations. The thermal variation of resistivity at higher temperatures tends to favor such a conclusion.

The resistivity of the pseudo-ternary alloy $Yb_2Al_{0.5}Mg_{0.5}Si_2$ is nearly temperature-independent between 300 and 200 K. It varies as $-\ln T$ as temperature decreases, peaks at around 20 K and then drops precipitously at lower temperatures. A distinct anomaly at 6.5 K close to the magnetic transition in this compound is noted. The $-\ln T$ variation of the resistivity, keeping also in view the resistivity behavior of Yb_2AlSi_2 and Yb_2MgSi_2, shows the presence of Kondo interaction in the mixed alloy. These results show that it is possible to track the evolution from spin fluctuating to trivalent magnetically ordered regime as x is varied from 0 to 1 in $Yb_2Al_{1-x}Mg_xSi_2$.

3.4. Heat capacity

The heat capacity of Yb_2MgSi_2 and $Yb_2Al_{0.5}Mg_{0.5}Si_2$ is shown in figure 7. The peak in the heat capacity clearly reflects the bulk magnetic transition at the respective T_N of the two compounds.

Since we do not have the data on non-magnetic, reference analog Lu_2MgSi_2, which would have given us a measure of the lattice heat capacity, we have estimated approximately the entropy associated with the magnetic transition by smoothly

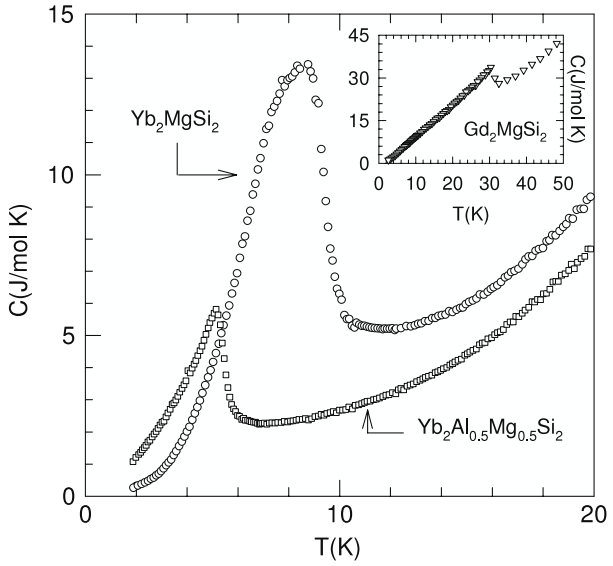

Figure 7. The heat capacity of Yb_2MgSi_2 and $Yb_2Al_{0.5}Mg_{0.5}Si_2$ between 1.8 and 20 K. The inset shows the heat capacity of Gd_2MgSi_2 between 1.8 and 50 K.

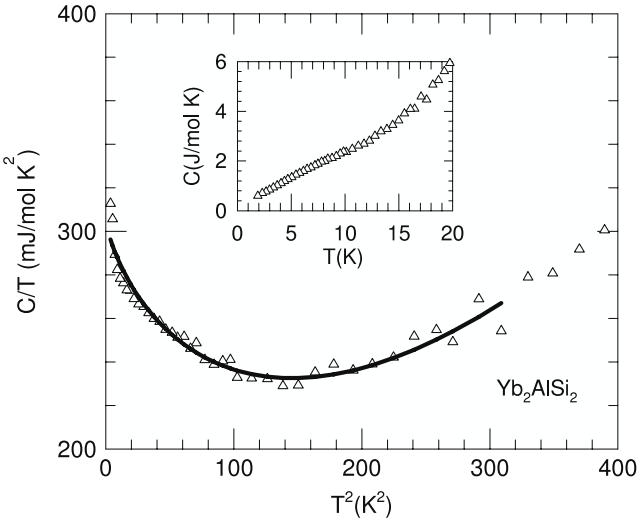

Figure 8. The plot of the heat capacity C/T versus T^2 of Yb_2AlSi_2 between 1.8 and 20 K. The solid lines are a fit of equation (1) to the data (see text). The inset shows the data in the form of C versus T.

extrapolating the low temperature C/T data to 0 K and the C/T plot above the magnetic transition to the intercept at 0 K. Following this procedure we obtain an entropy of nearly 4 and 1.9 J/Yb mol K in Yb_2MgSi_2 and $Yb_2Al_{0.5}Mg_{0.5}Si_2$, respectively. These values are less than $R\ln 2$, expected for a doublet $S = 1/2$ ground state, by 30% and 67% respectively in the two compounds. Reduced entropy in the magnetically ordered state often arises due to the presence of short range order above T_N. An additional mechanism due to the partial quenching of the Yb magnetic degrees of freedom by Kondo screening may also be operative, particularly in $YbAl_{0.5}Mg_{0.5}Si_2$.

The inset of figure 7 shows the heat capacity of Gd_2MgSi_2 which orders magnetically at 31 K. De Gennes scaling predicts the magnetic ordering temperature of a Yb analog in an isostructural series of rare earth compounds to be about 1% of the Gd compound, thus suggesting a magnetic transition temperature of ∼0.3 K in Yb_2MgSi_2. Therefore, the experimental T_N of 9.5 K implies a huge enhancement of the magnetic ordering temperature in Yb_2MgSi_2.

The heat capacity of Yb_2AlSi_2 is shown in figure 8 in the form of C/T versus T^2. The inset shows the heat capacity C is monotonically decreasing with temperature T down to the lowest data point of 1.8 K in our experiment. However, the C/T plot shows an interesting upturn below about 12 K. An upturn in C/T can be observed as a precursor to a magnetic transition but, since C does not show any upturn down to 1.8 K, a *magnetic* origin of the upturn can safely be ruled out. Besides, the magnetization data in figure 2 show convincingly that Yb_2AlSi_2 is a paramagnet. On the other hand, both the magnetization and resistivity suggest the presence of spin fluctuations in Yb_2AlSi_2. The paramagnon model [8–10] of spin fluctuations in exchange-enhanced paramagnets and nearly ferromagnetic materials predicts an additional contribution of the form $T^3\ln(T/T_{sf})$ to the electronic heat capacity for $T \ll T_{sf}$, where T_{sf} is the spin fluctuation temperature, such that the expression for the total heat capacity is given by

$$C = \gamma T + \beta T^3 + \delta T^3 \ln(T/T_{sf}) \qquad (1)$$

where the first two terms represent the usual electronic and lattice contributions to the heat capacity. Some of the well-known materials in which a $T^3\ln(T/T_{sf})$ contribution to the heat capacity has been observed are UAl_2 [11, 12], $TiBe_2$ [13], the heavy fermion superconductor UPt_3 [12, 14], $CeSi_x$ [15] and Ni_3Al [16]. The solid line in figure 8 shows that expression (1) provides a reasonably good fit to the data. The γ and T_{sf} values obtained by fitting are 305 mJ mol^{-1} K^{-2} and 24.5 K, respectively. An independent estimate of γ based on the phenomenological Kadowaki–Woods relation $A/\gamma^2 = 10^{-5}$ $\mu\Omega$ cm, obeyed by a host of heavy fermion valence/spin fluctuating compounds [7], gives $\gamma = 345.7$ mJ mol^{-1} K^{-2} using the values of A as derived from the resistivity data. Overall, there is a fairly good correspondence between the magnetization, heat capacity and resistivity data, strengthening the inference of a $T^3\ln(T/T_{sf})$ contribution to the heat capacity in Yb_2AlSi_2.

We have also fitted the expression $C = \gamma T + \beta T^3 + D$ to the data, where D represents a contribution due to the magnetic clusters which is constant for $T \gg T_A$, where $T_A = E_A/Sk_B$ (E_A is the average anisotropy energy of the cluster and S its spin) [17]. For the same fitting range as used for equation (1) above the fitting is very poor. However, for $T \leqslant 10$ K, the fit is even better than that based on the paramagnon model, but the fitted value of the coefficient of the lattice heat capacity β is negative, which is physically untenable. We therefore discard the magnetic clusters-based fit as meaningless for Yb_2AlSi_2.

3.5. ^{170}*Yb Mössbauer data*

3.5.1. Yb_2MgSi_2. We have supplemented the bulk thermodynamic and transport data described above with the

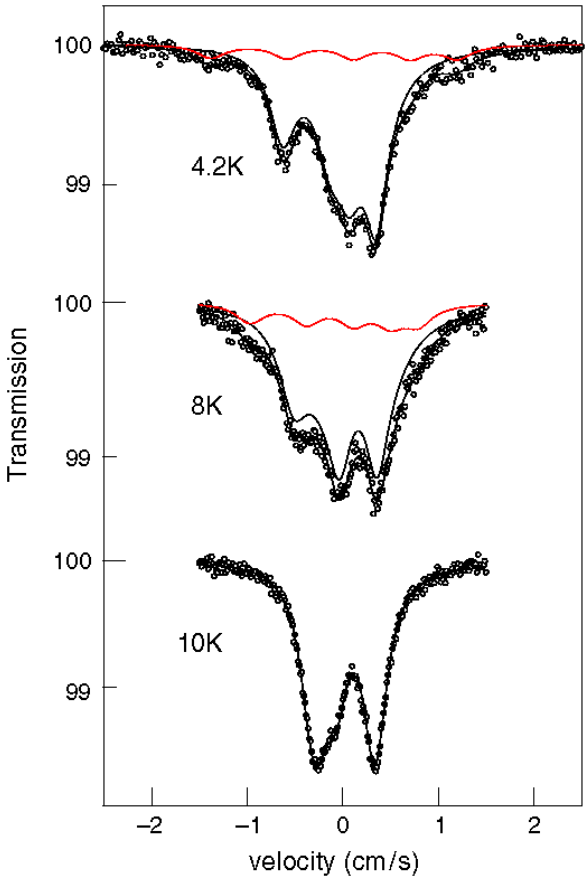

Figure 9. The ^{170}Yb Mössbauer spectra in Yb_2MgSi_2 at 4.2, 8 and 10 K. The red curve is the subspectrum (15% relative intensity) whose precise origin is not clear.

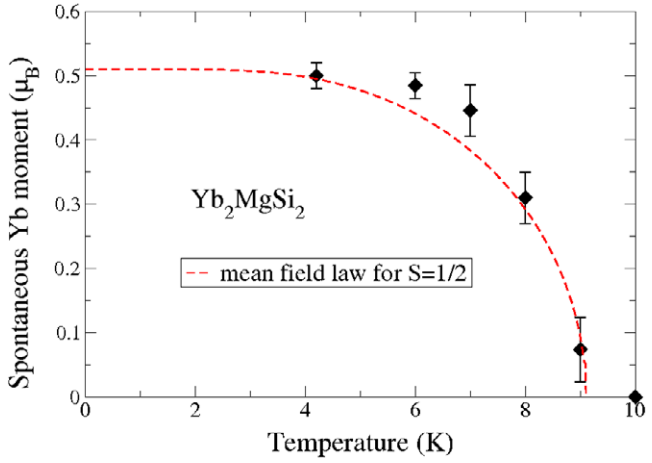

Figure 10. Thermal variation of the Yb spontaneous moment in Yb_2MgSi_2. The red dotted line is a mean-field calculation for $S = 1/2$, appropriate for a Kramers doublet, with $T_N = 9.1$ K.

microscopic technique of ^{170}Yb Mössbauer spectroscopy. The technique is based on the γ-ray resonant absorption between the ground nuclear state, with spin $I_g = 0$, and the first excited state, with spin $I = 2$, at an energy 84.3 keV.

Mössbauer spectra in Yb_2MgSi_2 were recorded in the temperature range 4.2–50 K (see figure 9). Below 10 K, the spectra show the presence of a magnetic hyperfine interaction and of a smaller quadrupolar hyperfine interaction; at 10 K and above, the quadrupolar interaction alone is present. These spectra show that magnetic ordering of Yb^{3+} moments occurs below 10 K, which is in agreement with the bulk thermodynamic and transport data presented above.

In the paramagnetic phase ($T \geqslant 10$ K), the spectrum is well accounted for by the quadrupolar hyperfine Hamiltonian in the excited nuclear state:

$$H_Q = \frac{eQV_{zz}}{8}\left[I_Z^2 - \frac{I(I+1)}{3} + \frac{\eta}{6}(I_+^2 + I_-^2)\right] \qquad (2)$$

where Q is the quadrupolar moment of the nuclear excited state, and V_{ZZ} and η are, respectively, the principal component and asymmetry parameter of the electric field gradient (EFG) tensor V_{ij} at the nucleus site. At 10 K, the fit of the spectrum to Hamiltonian (2) yields a quadrupolar parameter $\alpha_Q = \frac{eQV_{zz}}{8} = 1.63(2)$ mm s^{-1} and $\eta \approx 0.65$. The non-zero value of η is in agreement with the non-axial character of the local symmetry (mm, i.e. two perpendicular mirror planes) at the Yb site. Due to this low symmetry, it is not possible to assess the position of the main axes of the EFG tensor. The above parameters do not change much up to 50 K.

In the magnetically ordered phase, the usual procedure is to diagonalize the whole hyperfine Hamiltonian in the main EFG axes. Then the hyperfine field has angles θ and ϕ in this frame. The total Hamiltonian is

$$H_{hf} = -g_n\mu_n \mathbf{I}\cdot\mathbf{H}_{hf} + H_Q \qquad (3)$$

where g_n is the nuclear gyromagnetic factor and μ_n is the nuclear Bohr magnetron. In principle, the quadrupolar parameters are little affected in the magnetically ordered phase with respect to the paramagnetic phase. Anyway, in the fits of the magnetic spectra, the parameter α_Q was left free but η was kept fixed at the value 0.65. The other parameters were the magnitude and orientation of the hyperfine field. A further complication arises in the magnetically ordered phase because of the presence of a small intensity (about 15%) extra subspectrum (red line in figure 9), whose precise origin is unclear. Its hyperfine field is substantially larger than that of the majority subspectrum, which we shall consider to correspond to the main Yb_2MgSi_2 phase. We shall postpone the discussion of this minority spectrum to the later portion of this section.

The results of the fits of the spectra in the magnetically ordered phase are summarized in figures 10 and 11. For rare earths, the hyperfine field is proportional to the magnetic moment to a good approximation. In the case of Yb^{3+}, the constant of proportionality is: $C = 102T/\mu_B$ [18]. Using the measured hyperfine field values, one can determine the moment values. At 4.2 K, the hyperfine field is 51(2) T, and thus the saturated spontaneous Yb moment is 0.51(0.02) μ_B. This value is much reduced with respect to the free-ion saturated moment value of 4 μ_B; this is a crystal field effect and it suggests that the Yb moment is directed along a hard magnetic axis as a consequence of exchange anisotropy, similar to the cases of YbNiSn [19] and YbNiBC [20]. The thermal

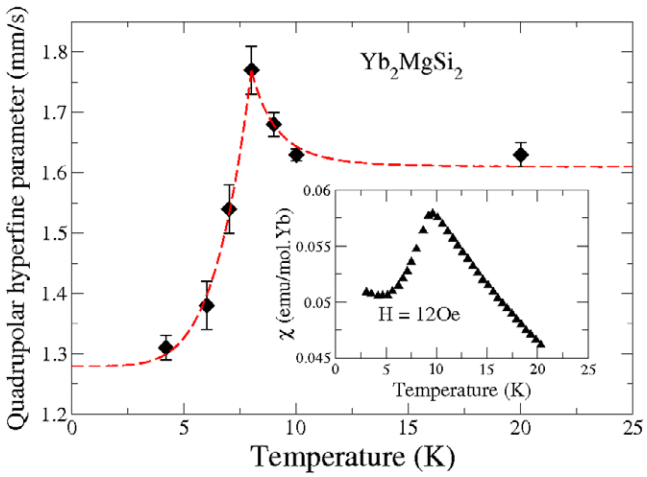

Figure 11. Thermal variation of the quadrupolar hyperfine parameter α_Q (the red line is a guide for the eye); inset: the peak in the magnetic susceptibility at 9.5 K.

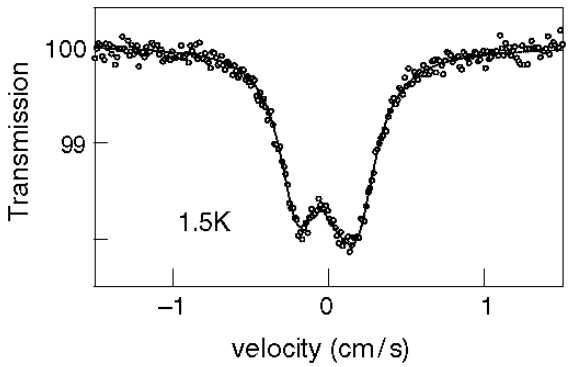

Figure 12. ^{170}Yb Mössbauer spectrum of Yb_2AlSi_2 at 1.5 K.

variation of the moment (figure 10) runs slightly above the expected mean field curve for an effective spin $S = 1/2$, which describes a well-isolated Kramers doublet, namely the ground state of Yb^{3+} in the crystal electric field. The orientation of the moment in the EFG tensor frame is: θ and $\phi \sim 90°$.

The thermal variation of the α_Q parameter (figure 11) is rather unexpected: it presents a peak at 8 K, very close to the magnetic transition ($T_N = 9.5$ K, see the inset of figure 11). Actually, α_Q (or $V_{ZZ}(T)$) is made of two contributions: a lattice contribution representing the electric field gradient arising from the charges surrounding the Yb site and a usually dominant 4f contribution arising from the distortion of the 4f shell itself by the crystal electric field. This latter contribution can be expressed as a function of the 4f quadrupolar moment $Q^{4f}_{ZZ} = \langle 3J_Z^2 - J(J+1)\rangle_T$, where J_Z is the component of the total angular momentum **J** ($J = 7/2$ for Yb^{3+}) along the principal axis OZ of the EFG tensor, namely $\alpha^{4f}_Q = B_Q Q^{4f}_{ZZ}$, B_Q being a hyperfine constant. The thermal variation of α_Q is entirely due to the 4f contribution. Usually, α_Q suffers a small jump at the magnetic transition, as the Yb wavefunctions lose the mixing with excited states due to the presence of an exchange field. The presence of a peak near T_N in its thermal variation may imply a strong coupling of the 4f quadrupolar moment with the magnetic moment through a magneto-elastic coupling [21]. Two other experimental features could be due to a strong magneto-elastic coupling: the 'squaredness' of the thermal variation of the moment and the high value of the Néel temperature (9.5 K) which is comparable to the highest ever recorded among Yb compounds.

3.5.2. The minority subspectrum. The minority subspectrum (15% relative intensity) visible in the magnetically ordered phase has a hyperfine field that decreases from 170 T at 4.2 K to 97 T at 9 K. Its presence is puzzling and has no clear explanation up to now. It could be a second Yb site in the Yb_2MgSi_2 magnetic phase, appearing because of a peculiar magnetic structure. However, the small fraction (about 1/6) of the Yb ions in this site makes this hypothesis very unlikely. Another possibility could be the presence of a Yb silicate impurity phase, where the recoil-free fraction of the Yb site is much larger than that of the main Yb_2MgSi_2 phase. This can occur if the atomic bonds in the impurity phase are much harder than in the main phase, leading to a much higher Debye temperature. Then, even a small Yb atomic fraction in the impurity phase (a few 0.1%) can lead to an approx. 10% spectral contribution. However, in our Yb_2MgSi_2 sample, no Yb oxide or silicate could be detected by x-ray diffraction and metallography. Though the origin of the minority subspectrum is not clear, it has no bearing on the intrinsic magnetic behavior of Yb_2MgSi_2.

3.5.3. Yb_2AlSi_2. Mössbauer spectra were recorded between 1.5 and 30 K. They are pure hyperfine quadrupolar spectra (see figure 12) with an almost temperature-independent $\alpha_Q \approx -0.95$ mm s^{-1} and $\eta \approx 0.7$. Mössbauer spectra thus confirm the paramagnetic nature of Yb_2AlSi_2, at least down to 1.5 K, and provide additional proof about the absence of any minor (impurity) magnetically ordered phase(s) in this compound.

It is interesting to note that, even though the unit cell volume of Yb_2AlSi_2 (193.4 Å^3) is smaller than that of Yb_2MgSi_2 (204.8 Å^3), the latter orders magnetically while the aluminide is paramagnetic. Typically a lower volume favors the trivalent magnetic configuration of the Yb ions as the ionic radius of Yb^{3+} is less than that of the non-magnetic Yb^{2+}. For example, $YbCu_2Si_2$ is a valence fluctuating compound but Yb ions in $YbCu_2Ge_2$ with a larger lattice volume are in the divalent state. It may be noticed that both Si and Ge are nominally isovalent atoms. Evidently, the extra electron donated by Al with an outermost electronic configuration of $3s^23p^1$ (compared to $3s^2$ of Mg) affects the electronic band structure such that the 4f conduction electron hybridization is enhanced substantially, resulting in a paramagnetic ground state even though the cell volume decreases with increasing Al content. It appears that the hybridization between the Yb 4f and conduction electrons, determined mainly by the position of the 4f level with respect to the Fermi level, is sensitively poised in these compounds. In ambivalent Yb compounds external pressure decreases hybridization and favors a magnetic Yb^{3+} state. For example, pressure studies on YbNiSn show that the magnetic transition

temperature T_c initially increases rapidly with $dT_c/dP = 0.3$ K kbar^{-1} [22]. In the present case a decreased volume induced by pressure may tend to favor a paramagnetic behavior as a lower volume in this particular structure type favors a paramagnetic ground state as observed in Yb_2AlSi_2. The intermediate composition alloy $Yb_2Al_{0.5}Mg_{0.5}Si_2$, with a lower lattice volume compared to Yb_2MgSi_2, orders magnetically at a lower temperature and its resistivity shows Kondo behavior. The thermal variation of the resistivity of Yb_2MgSi_2 indicates spin fluctuations at high temperatures though the compound orders magnetically at 9.5 K. Therefore, it would be interesting to see how these compounds respond to externally applied pressure.

The heat capacity of Yb_2AlSi_2 shows an interesting upturn which is tentatively explained by the inclusion of a $T^3 \ln(T/T_{sf})$ term in the electronic heat capacity. Such a contribution was predicted by the paramagnon model, first put forward to explain the absence of s-wave singlet superconductivity in Pd [8]. The paramagnon model also predicts that the spin fluctuations can be quenched by the application of a magnetic field with energy comparable to $k_B T_{sf}$, resulting in a reduced electronic specific heat [23–25]. In this regard, measurement of the heat capacity of Yb_2AlSi_2 to lower temperatures and in high applied fields would be interesting. It may also be worthwhile to replace Al by Mg at low levels to find whether a quantum critical point is induced without the introduction of too much disorder in the system.

To conclude, our studies on $Yb_2Al_{1-x}Mg_xSi_2$ ($x = 0$, 0.5 and 1) show that the Yb 4f conduction electron hybridization varies drastically with x. Yb_2MgSi_2 orders magnetically with a relatively high T_N of 9.5 K but Yb_2AlSi_2 exhibits a Pauli paramagnetic ground state due to a strong Yb 4f conduction band mixing. At an intermediate composition of $Yb_2Al_{0.5}Mg_{0.5}Si_2$ magnetic ordering and Kondo interaction co-exist.

References

[1] Krahnenberg C and Mewis A 2000 *Z. Anorg. Allg. Chem.* **626** 1448
[2] Kraft R and Pottgen R 2005 *Monatsh. Chem.* **136** 1707
[3] Dhar S K, Manfrinetti P and Palenzona A 1997 *J. Alloys Compounds* **252** 24
[4] Yvon K, Jeitschko W and Parthe E 1977 *J. Appl. Crystallogr.* **10** 73
[5] Buschow K H J and van Daal H J 1972 Magnetism and magnetic materials *AIP Conf. Proc.* **5** 1464
[6] Mattens W C M 1980 *Thesis* Amsterdam University
[7] Kadowaki K and Woods S B 1986 *Solid State Commun.* **58** 507
[8] Berk N F and Schrieffer J R 1966 *Phys. Rev. Lett.* **17** 433
[9] Doniach S and Engelsberg S 1966 *Phys. Rev. Lett.* **17** 750
[10] Rice M J 1967 *Phys. Rev.* **159** 153
[11] Trainor R J, Brodsky M B and Culbert H V 1975 *Phys. Rev. Lett.* **34** 1019
[12] Frings P H and Franse J J M 1985 *Phys. Rev.* B **31** 4355
[13] Stewart G R, Smith J L and Brandt B L 1982 *Phys. Rev.* B **26** 3783
[14] Stewart G R, Fisk Z, Willis J O and Smith J L 1984 *Phys. Rev. Lett.* **52** 679
[15] Dhar S K, Gschneidner K A Jr, Lee W H, Klavins P and Shelton R N 1987 *Phys. Rev.* B **36** 341
[16] Dhar S K and Gschneidner K A Jr 1989 *Phys. Rev.* B **39** 7453
[17] Hahn A and Wohlfarth E P 1968 *Helv. Phys. Acta* **41** 857
[18] Bonville P, Imbert P, Jéhanno G, Gonzalez-Jimenez F and Hartmann-Boutron F 1984 *Phys. Rev.* B **30** 3672
[19] Bonville P, Bellot P, Hodges J A, Imbert P, Jéhanno G, LeBras G, Hammamm J, Leylekian L, Chevrier G, Thuéry P, D'Onofro L, Hamzic A and Barthélémy A 1992 *Physica* B **182** 105
[20] Bonville P, Hodges J A, Hossain Z, Nagarajan R, Dhar S K, Gupta L C, Alleno E and Godart C 1999 *Eur. Phys. J.* B **11** 377
[21] Morin F and Schmitt D 1990 *Ferromagnetic Materials* vol 5, ed K H J Buschow and E P Wohlfarth (Amsterdam: Elsevier) p 5
[22] Sparn G, Thompson J D and Hamzic A 1992 *J. Alloys Compounds* **181** 197
[23] Brinkman W F and Engelsberg S 1968 *Phys. Rev.* **169** 417
[24] Béal-Monod M T, Ma S-K and Fredkin D R 1968 *Phys. Rev. Lett.* **20** 929
[25] Béal-Monod M T and Daniel E 1983 *Phys. Rev.* B **27** 4467